Int. J. Nanosci. Nanotechnol., Vol. 9, No. 1, March 2013, pp. 39-50

Modeling of Air Relative Humidity Effect on Adhesion Force in Manipulation of Nano-Particles and its Application in AFM

M. H. Korayem*, Z. Rastegar, A. H. Korayem, A. E. Heidari

Robotic Research Laboratory, School of Mechanical Engineering, Iran University of Science and Technology, Tehran, I. R. Iran

(*) Corresponding author: hkorayem@iust.ac.ir
(Received:10 Dec. 2012 and Accepted: 23 March 2013)

Abstract:
In this paper, the effect of air relative humidity and capillary force on contact geometry of surfaces based on JKR model by Atomic force microscopy was investigated in order to manipulate nano-particles. With transition from macro to nano-scale, the effect of surface forces becomes more significant in comparison with inertial force. Because contact mechanics models are based on surface energy and there is a permanent humidity in surrounded environment. In order to precisely determine the forces in AFM dynamics equations and different environments and also their application in contact modeling, the effect of capillary forces must exactly be specified. Experimental results showed that the air relative humidity percentage affects the adhesion force. So, as AFM is used for fine and nano-scale particles. These forces have significant effect on operation accuracy and should not be neglected. In this paper, the effect of capillary forces has been modeled based on JKR contact mechanics model. The results obtained from this modeling have been compared with experimental data.
Keywords: *AFM, Nano-manipulation, Relative humidity, Capillary force, Adhesion force, Contact models.*

1. INTRODUCTION

Nano-manipulation can be defined as manipulation of nano-scale pieces with nano-size end-effectors. Manipulation includes pulling, pushing and tracking, indenting, cutting, assembling, bending and twisting nano-scale pieces with external forces controlled by sensory feedbacks [1].
Manipulation method based on atomic force microscopy (AFM) is developing. The main factors of determining macroscopic characteristics of materials are the forces exist among their microscopic elements [8]. In this paper, AFM has been used as an equipment to exert the force on particles in order to displace (or manipulate) them. So, all of the forces between tip and particle should be specified in order to have more accurate equations and consequently more precise manipulation. Since important forces in nano-scale and also tip-particle interaction in different environments are not completely determined, this process is still underdeveloped. Interface forces can deform particles in the same way as external forces do [11].
In order to predict indentation depth and contact radius, different contact mechanics models such as Hertz, JKR (Johnson, Kendall, and Roberts), DMT (Derjaguin, Muller and Toporov), MD (Maugis and Dugdale) and Schwartz have been predicted. In the JKR model which represented by Johnson, Kendall

and Roberts, the geometry of contact has been calculated by considering surface forces, while the effect of relative humidity on capillary and pull-off forces has been ignored [14]. Dynamic modeling is a fundamental tool for realization of nano-manipulation process. In this case nano-particle can be tracked every instant. So, scientists can put a nano-particle in an appropriate place in order to manufacture or assemble in micro/nano scale. Kim, Tafazzoli, Sitti and Falvo have worked in this field [1-4].

In most researches and experiments, some of forces (for example, capillary force) have been ignored in order to make it simpler. The environment always contains humidity and this factor can affect the mechanical and adhesional properties of the most materials. Therefore, the effects of humidity should be considered, especially in nano-scale particles [7]. Previous studies showed that when particle size is greater than 1μm or humidity is low, relative humidity has no significant effect on capillary force and the effect of this force may be neglected [9].

Jones et al. studied the pull-off forces between flat glass or silicon surfaces and silicon AFM tips or glass microspheres of different sizes as a function of relative humidity (RH) in the range of 5−90%, as model systems for the behavior of cohesive powders using AFM. The glass and silicon substrates were treated to render them either hydrophobic or hydrophilic.

All the hydrophilic surfaces gave simple force curves and pull-off forces increasing uniformly with RH. Small contacts (R ~ 20 nm) gave pull-off forces close to values predicted by simple Laplace−Kelvin theory (~20 nN). However, the values with microspheres (R ~20 μm) fell well below predictions for sphere−flat or sphere−sphere geometry, due to roughness and asperity contacts. The hydrophobic silicon surfaces also exhibited simple behavior, with negligible RH dependence.

The pull-off force again fell well below predicted values (Johnson−Kendall−Roberts contact mechanics theory) for the larger contacts [15]. Since in this paper the tip and the particle are nano-sized, surface forces should completely be considered in order to precisely determination of dynamic equations and consequently pull-off force of surfaces [10].

For the systems in contact, such as AFM tip and sample surface, an aqueous bridge would be formed between two solid bodies. This bridge causes an adhesion force which its value depends on contact angle between water and surface, humidity and accurate geometry of aqueous bridge [6].

Different geometrical models for capillary force have been presented by different researchers such as Chen, Farshchi, Paajanen, Pakarinan and Sirghi [5-9]. Chen proposed a more complete model for capillary force based on geometry and equivalent forces in water-air interface for calculation of adhesion force. He showed that in low percentage of humidity, the pressure force is a main factor, while in high humidity the adhesion force is a main factor in capillary force [5].

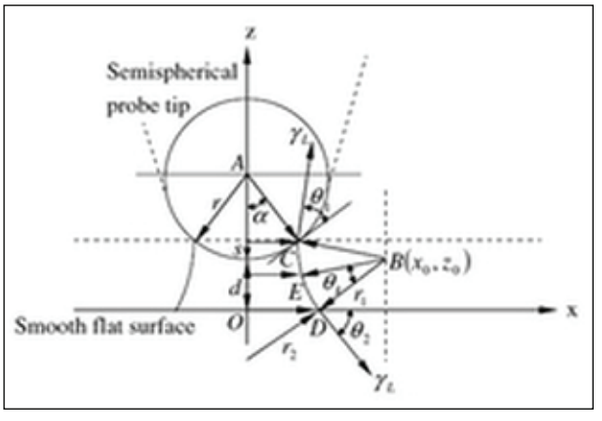

Figure 1: *Schematic diagram of liquid bridge between a flat surface and probe [5]*

2. CAPILLARY FORCE

There are two basic methods for obtaining (or for evaluation of) the capillary force. If there is a drop between two solid bodies (griper and pieces), it will be deformed to an arc (liquid bridge). The other situation would be developed of capillary bridge because of condensation of environment humidity in the pores between two rough surfaces in contact. In both conditions this phenomenon can be explained as shown in Figure 1.

The characteristics of this liquid bridge can be defined by volume (V), surface tension (γ), and surface wet ability defined by contact radii θ_1 and θ_2. Considering that the contact radii of the surfaces are identical ($\theta_1=\theta_2=\theta$), the volume is constant and the immersion height (D^0) is low, the capillary force between a surface and a sphere with radius of R can be simplified as:

$$F_c = \frac{4\pi R\gamma \cos\theta}{1+(D/d)} \tag{1}$$

2.1. Chen capillary force model

Using the geometry shown in Figure 1, for a spherical particle, capillary pressure force and surface tension force are as follows:

$$Fp = -\pi\left(R_a \sin\alpha\right)^2 \frac{\gamma_l}{r_k} \tag{2}$$

$$F_{st} = -2\pi R_a \gamma_l \sin\alpha \sin(\alpha+\theta_1) \tag{3}$$

Where:

$$R_a = R_1R_2 / R_{1+}R_2$$

α: The angle of lateral axis and radius vector which mentions the transaction between probe tip and liquid bridge.

θ_1: The angle of probe tip and liquid bridge.

3. CONTACT MECHANICS THEORIES

3.1. JKR model

When surface forces have short-range in comparison with elastic deformation of contact, the JKR model can be used with good approximation. However, for a hard material, weak adhesion forces and fine particles, surface forces out of contact area can be ignored. Total energy, U_T, can be obtained as:

$$U_T = U_E + U_M + U_S = \frac{1}{K^{\frac{2}{3}}R^{\frac{1}{3}}}\left[\frac{1}{15}P_1^{\frac{2}{3}} + \frac{1}{3}P_0^2P_1^{-\frac{1}{2}}\right] - \frac{1}{K^{\frac{2}{3}}R^{\frac{1}{3}}}\left[\frac{P_0P_1^{\frac{2}{3}}}{3} + \frac{2}{3}P_0^2P_1^{-\frac{1}{2}}\right] - \gamma\pi\frac{R^{\frac{2}{3}}P_1^{\frac{2}{3}}}{K^{\frac{2}{3}}} \tag{4}$$

The equilibrium can be obtained when:

$$dU_T / da_1 = 0$$
$$dU_T / dP_1 = 0 \tag{5}$$

The required force in order to separate two surfaces is perpendicular to contact surface. Using JKR model, the contact radius and the indentation depth will be:

$$a^3 = \frac{R}{K}\left(P + 3\gamma\pi R + \sqrt{\left\{6\gamma\pi RP + \left(3\gamma\pi R\right)^2\right\}}\right) \tag{6}$$

$$\delta = \frac{a^2}{R} - \sqrt{\frac{8\pi\gamma a}{3K}} \tag{7}$$

Where, $F=F_t$ and $R' = \frac{R_tR_p}{R_t+R_p}$ in tip-sample contact, and $F = F_s$ and $R' = R_p$ for sample-substrate contact.

These deformations are important in nano scale because of particle size. In macro systems, however, the adhesion force may be neglected in comparison with pushing force.

3.2. Schwartz theory

A new method has been presented by Schwartz to calculate elastic deformation of a sphere on a flat surface. In this model, in addition to long-range forces, the effect of short-range attraction forces has been considered. Unlike previous models, the characteristics of these deformations have been explained for JKR and DMT. Some equations for calculation of contact radius and pressure distribution of deformation have been represented. In all equations the critical force which may be found between JKR and DMT values, acts as a transition parameter.

In this paper, Hertz equivalent load (F_H) is defined as a force which should explain equation (7). For example, to obtain real contact radius (a), Hertz equivalent load can be considered as an effective applied load including adhesion distribution. Johnson et al. showed that F_H^{jkr} increases Hertz equivalent load which is greater than external applied load F_T.

In Schwartz theory, by considering long-range force $(2\pi r w_2)$ and replacing external force by $F = F + 2\pi r w_2$, the Hertz equivalent load will be calculated by the following equation, based on JKR model:

$$F_H^{JKR} = F + 2\pi r\omega_2 + 3\pi r\omega_1 \pm \sqrt{6\pi r\omega_1(F + 2\pi r\omega_2) + (3\pi r\omega_1)^2} \quad (8)$$

4. MODELING OF CAPILLARY FORCE

4.1. Based on JKR theory

Mechanical and adhesional properties of materials are sensitive to even low values of vapor in environment. For example, powder adhesion, quartz hardness and rocks' properties obviously depend on relative humidity. All of these effects depend partly on water capillary condensation around contact areas [12].

In equations (6 and 7) contact geometry have been calculated considering only Van der Waals forces. So, in order to have more accurate equations and considering effective forces, the generalized JKR relation considering capillary force and the variation of Kelvin radius is presented in this paper. So the effects of air relative humidity and Kelvin radius on contact geometry can be investigated using this method. Equation (2) involves Kelvin radius and consequently variation of relative humidity. So obtaining the energy causing by this force and adding to equation (3) will apply variation of relative humidity simultaneously in both prediction of contact radius and indentation depth. As mentioned before, adhesion force due to capillary force has two parts, surface tensile force and the force due to Laplace pressure. In this modeling (based on Chen model), the α angle can be calculated. So the variation of contact radius with respect to variation of humidity can be specified more accurate. This variation is more complete in comparison with Paajanen model.

By considering these two terms, the energy can be calculated by equations (11) and (12).

$$U_P = -\int F_p . d\delta \quad (9)$$

δ parameter can be defined as: a R, so:

$$U_P = -\frac{\pi\gamma_l}{r_k} a^2 R_a \sin^2\alpha \quad (10)$$

Substituting (a) in to equation 10:

$$U_P = -\frac{\pi\gamma_l}{r_k} R_a \sin^2\alpha \left(\frac{RP}{K}\right)^{2/3} \quad (11)$$

$$U_{st} = -2\pi\gamma_l \sin\alpha \sin(\alpha + \theta_1).a^2 \quad (12)$$

Equilibrium condition is $\frac{dU_T}{dp_1} = 0$. So the equation will be as follows:

$$\frac{dU_T}{dP_1} = \frac{P_1^{\frac{-4}{3}}}{9K^{\frac{2}{3}}R^{\frac{1}{3}}}\left[P_1^2 - P_0^2 - 2P_1P_0 + 2P_0^2 - 6\gamma\pi RP_1\right] - \frac{2}{3}\frac{\pi\gamma_l}{r_k}.R_a \sin^2\alpha \left(\frac{R}{K}\right)^{2/3} p_1^{-1/3} - \frac{4}{3}\pi\gamma_l \sin\alpha \sin(\alpha + \theta_1)\left(\frac{R}{K}\right)^{2/3} p_1^{-1/3} \quad (13)$$

As it shown, the parameter r_k has been applied in new equation (equation 13), which contains capillary radius and humidity variation. So, contact radius variation and consequently surfaces pull-off force according to relative humidity can be calculated. Since AFM tip and particle were considered to be spherical in this paper, R_a has been calculated as an equivalent radius of two spheres.

5. MANIPULATION OF NANO-PARTICLES BASED ON AFM IN AIR

Dynamic modeling is a fundamental tool for realization of nano-manipulation process and in this case nano-particle can be tracked every instant which make scientists capable of putting nano-particle in an appropriate place in order to manufacture or assemble in micro/nano scale.

In this article nano-particles with the radius of R_p which have been observed in substrate are pulled by AFM in environmental condition. AFM manipulation tool involves a cantilever and a conical

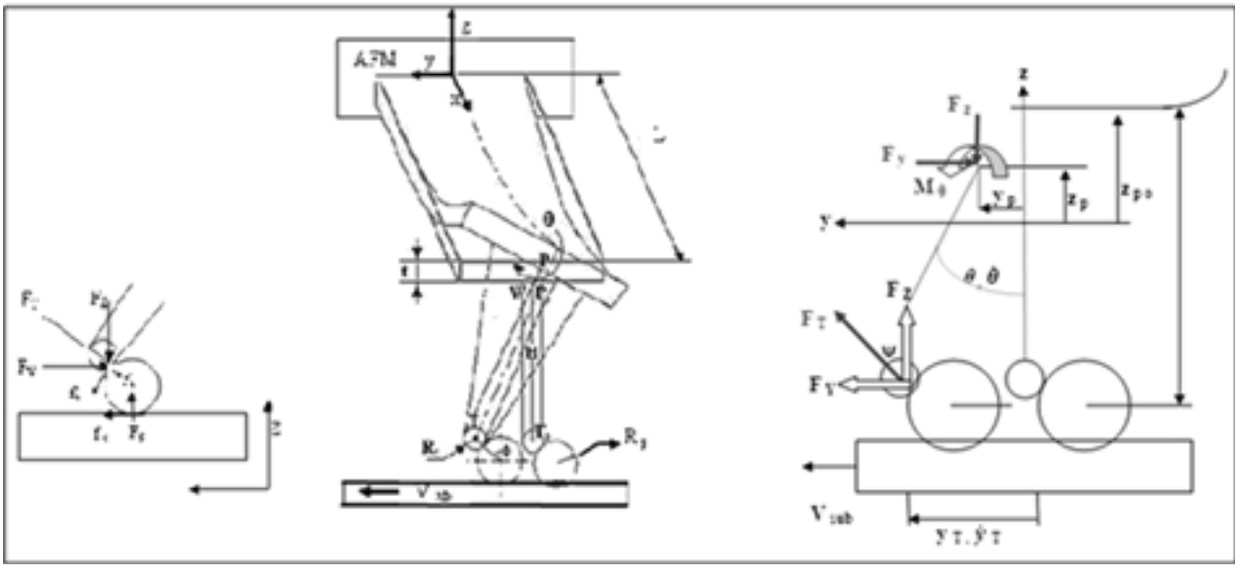

Figure 2: (a) *The deformation of the Cantilever in lateral movement and applied forces on tip of probe,* ***(b)*** *Applied forces on probe tip,* ***(c)*** *Free diagram of particle movement [13].*

probe which their geometry and size is shown in Figure 2(a). Cantilever dimensions in x, y and z directions are specified by L, W and t, respectively. The probe has the height of H. In order to do micro/nano manipulation and assembly, first imaging of substrate and observed particles will be done. Then to do micro/nano manipulation and assembly, the AFM tip will contact with micro/nano scale particle and move it on substrate.

Moving of tip or substrate with the constant velocity of V_{sub} leads to increasing the applied load by nano-manipulator on particle F_T to critical value of F_{Cr} to overcome adhesion forces and hereafter particle movement on substrate will start .The reaction force leads to bending and twisting of cantilever (Figure 2(a)).

Before particle movement on substrate, the input of problem is the particle position ,and the output is the applied force by tip on particle F_T. By increasing the force to its critical value in which the particle starts to move, F_T becomes constant and particle will move on substrate .The output of this part will define dynamic behavior and displacement of the particle.Considering contact deformation between tip-particle δ_t and particle-substrate, δ_s kinematic equations for cantilever deformation will be obtained as follows (Figure 3).

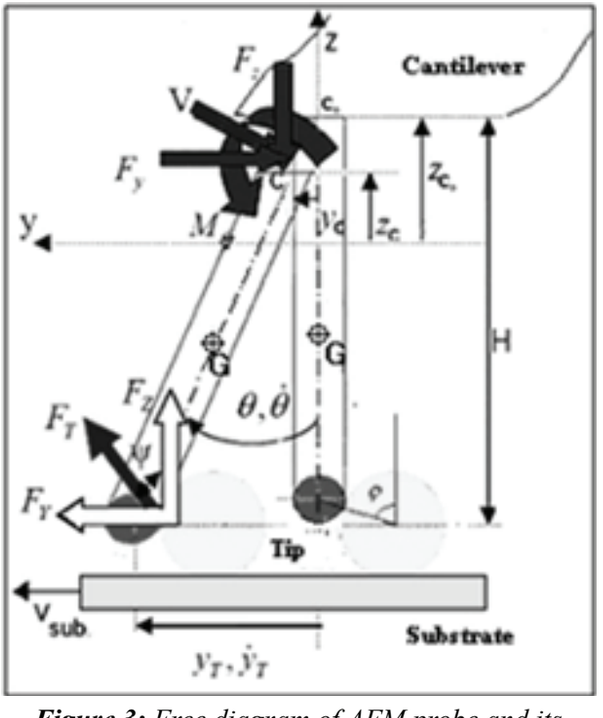

Figure 3: *Free diagram of AFM probe and its forces[3]*

The applied forces and momentums at the end of

cantilever will be as follows:[3]

$$F_Y = F_y \sin^2\theta - F_z \cos\theta \sin\theta + \frac{M_\theta \cos\theta + I_p \ddot{\theta} \cos\theta}{H} + \frac{m \sin\theta}{2}(\ddot{y}_T \sin\theta + \ddot{y}_P \sin\theta - \ddot{z}_T \cos\theta - \ddot{z}_P \cos\theta) \quad (14)$$

$$F_Z = F_z \cos^2\theta - F_y \cos\theta \sin\theta + \frac{M_\theta \sin\theta + I_p \ddot{\theta} \sin\theta}{H} - \frac{m \cos\theta}{2}(\ddot{y}_T \sin\theta + \ddot{y}_P \sin\theta - \ddot{z}_T \cos\theta - \ddot{z}_P \cos\theta) \quad (15)$$

And finally F_T and ψ can be obtained as:

$$F_T = \sqrt{F^2{}_Y + F^2{}_Z} \quad (16)$$

$$\psi = \tan^{-1}(\frac{F_Y}{F_Z}) \quad (17)$$

6. SIMULATION OF THE EFFECTS OF AIR HUMIDITY AND CAPILLARY FORCE ON MANIPULATION OPERATION

In this section, the effects of air humidity, capillary force, contact angle and particle size on contact geometry and manipulation operation is simulated. Then the value of the applied load by manipulator F_{cr} and variation of critical time T_{cr} for particles with different radii and materials will be simulated. The results are compared with gas environment. Simulations have been carried out using equations (9-13), Schwartz method and Matlab software. Finally the results of two methods have been compared. The parameters used in this simulation are:

$$\gamma_l = .0728 \ \ j/m^2, \ \ \gamma_s = .2 \ \ j/m^2 \ , \ \ K = 8548 \times 10^7 ,$$

$$\theta_1 = \theta_2 = 30°, R_1 = 20\,nm \ \ , R_2 = 50\,nm$$

6.1. Capillary force effect on contact mechanics

Using Kelvin equation,variation of the radius r_k with respect to relative humidity (p/ps) is shown in Figure 4. The humidity ranged from 10 to 90 percent and the variation of r_k is observed. As shown in this Figure, increasing the relative humidity leads to exponential increase in Kelvin radius. For greater percentage of humidity, its growth is more significant.

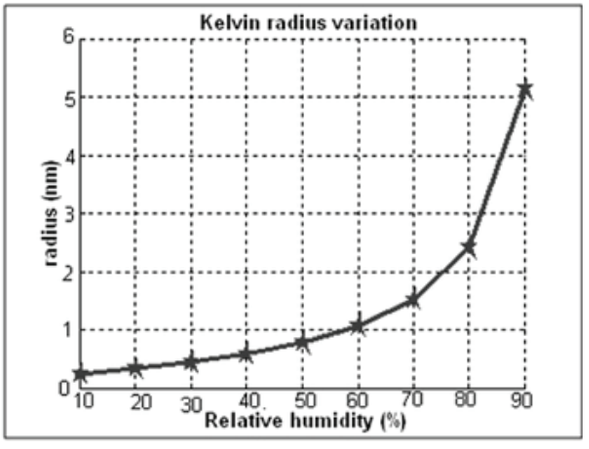

Figure 4: *Radius Vs. relative humidity*

According to equation (16), extracting a new P and substituting it into $a_1^3 = RP_1/K$ gives the plot of new contact radius vs. humidity. As shown in Figure 5, by increasing the humidity and therewith greatening of capillary bridge, the contact radius increases. So it may be concluded that the humidity results in increasing of adhesion and consequently contact radius growth. These results are in agreement with experimental data presented by Chen in which adhesion energy increases by increasing the humidity.

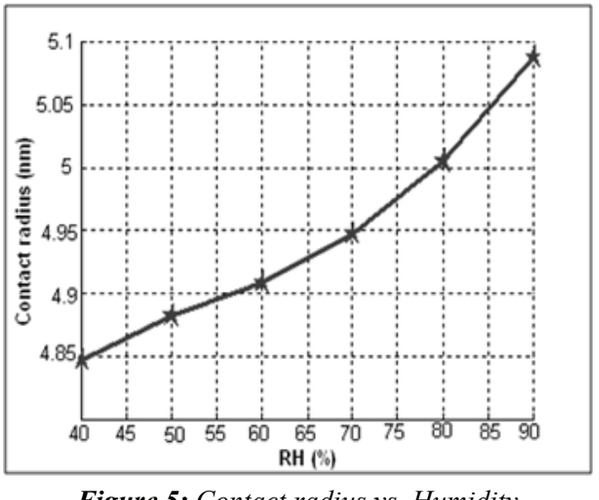

Figure 5: *Contact radius vs. Humidity*

It is worth to observe the variation of the contact

radius with respect to the applied load ranged from 0 to 10^{-8}N. As shown in Figure 6, by increasing the applied load the contact radius becomes larger. In addition, the rate of increasing of the contact radius increases by increasing the humidity percentage. The results of the presented model are compared with Experimental data carried out by Johnson. It should be noted again that Johnson has neglected from capillary force in his calculation

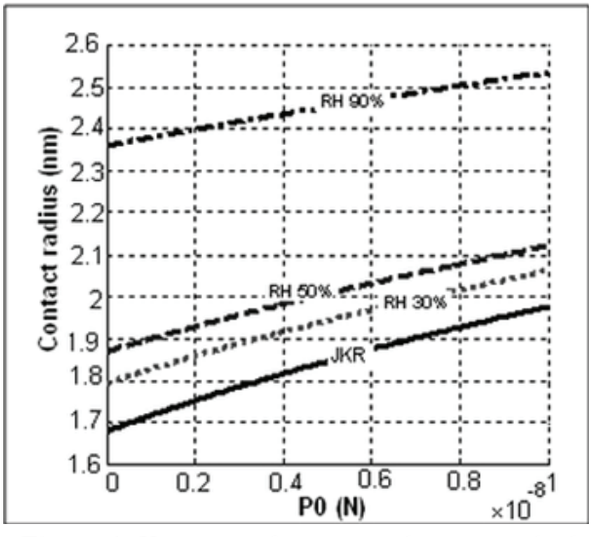

Figure 6: *Variation of contact radius vs. applied load. Contact radius increases considering capillary term in the relevant equations*

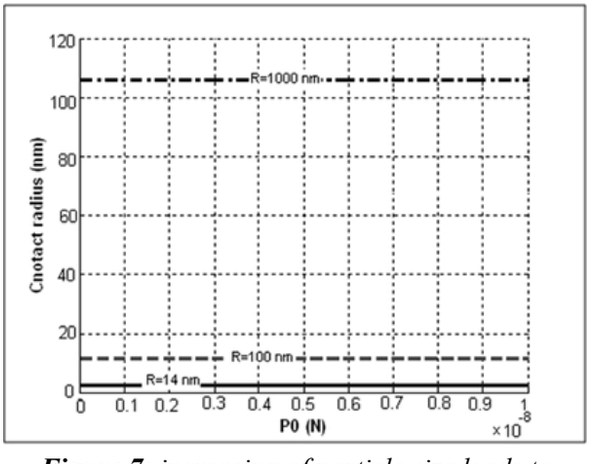

Figure 7: *increasing of particle size leads to increasing the contact radius*

The lowest curve is the Johnson curve which is plotted regardless of capillary term. As shown in Figure 6, considering capillary term in equations will increase contact radius which grows with increasing of humidity percentage. In Figure 7 contact radius variations for particles with different radii have been plotted. Obviously, greater particles will have larger contact area. So increasing the particle size will increase contact radius.

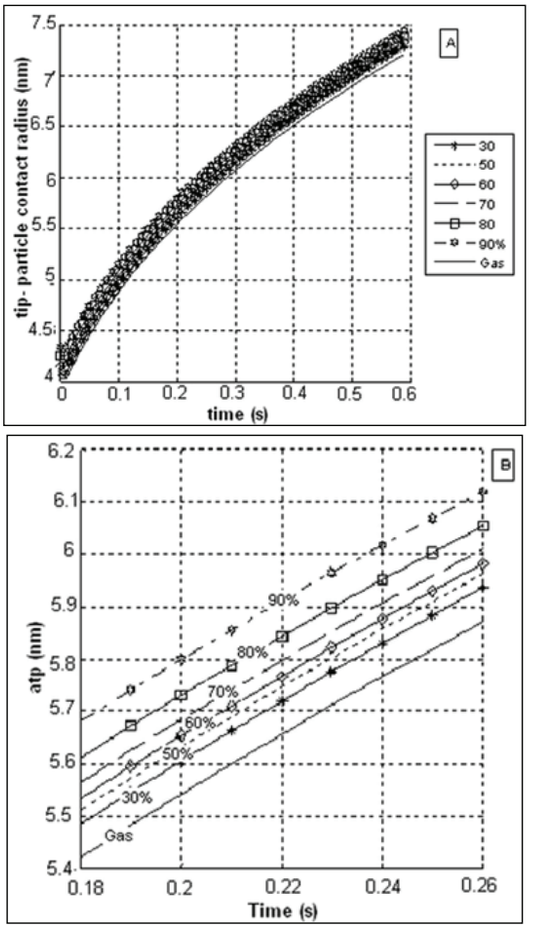

Figure 8: *(a) Tip-particle contact radius increases by time, increasing of humidity and tip force (b) Magnified curve of part (a)*

6.2. Capillary force effect on geometry of manipulation contact

Contact area and indentation depth curves for the particle with dimension of $a_p = 50nm$ and the tip with radius of $a_{tip} = 20nm$ have been drawn in Figure 8. According to equations (9-13), capillary force has been considered in equations. Its effect in different humidity percentage has been investigated

and compared with vacuum environment which has no humidity. As shown in Figure 8, inserting capillary force results in increasing of tip-particle contact radius (a_{tip}) and humidity growth will increase this value. Also time and increasing of tip force have increased the contact radius.

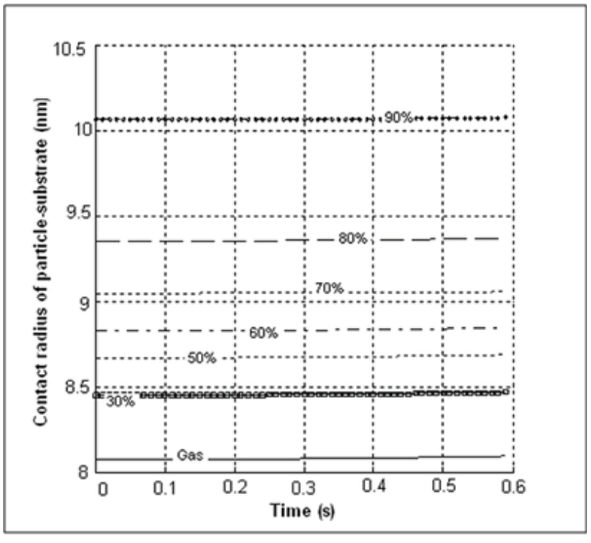

Figure 9: *Humidity percentage growth results in increasing of* a_{sub} *but time has no significant effect.*

Figure 10 shows humidity effect on contact radius of particle-substrate a_{sub}. Time has not significant effect on this contact area, while increasing of humidity percentage will increase it.

Characteristics of manipulation contact geometry are investigated again for particles with the dimensions of $1\mu m$, $500nm$.

As shown in Figures 10 and 11, increasing the particle radius leads to contact radius growth. This situation for different humidity percentages is the same as before, it means that increasing of humidity percentage results in greater growth.

6.3. Capillary force effect on manipulation process based on JKR model

Using Figure 13 diagrams, the transaction of two forces is at $t = 0.2$ and the point value is $F_T = 8.394 \times 10^{-7}$.

Now, capillary force is considered in equations and Relative humidity variation effect on these two forces transaction point and therefore manipulation start point is investigated. As shown in Figure 14, the manipulation start point increases with humidity percentage growth, because capillary force in addition to other forces has been inserted in equations so manipulation happens with delay. Figure 14 shows manipulation start point variation with humidity percentage growth.

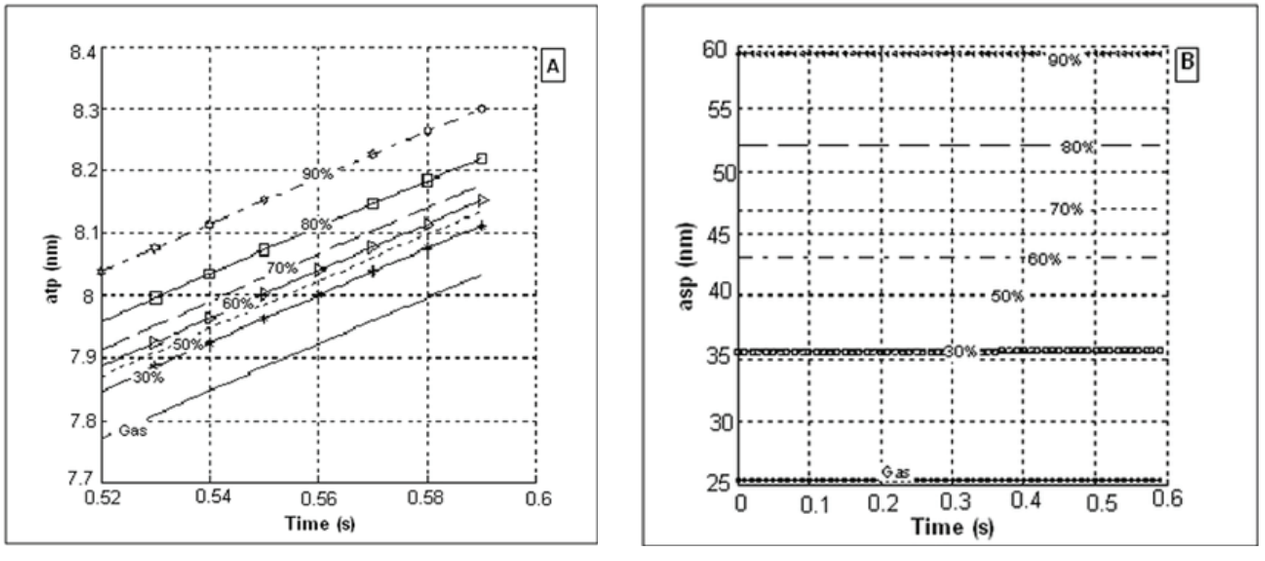

Figure 10: *Geometrical properties of (a) tip-particle, (b) particle-substrate for particle of size* $500nm$

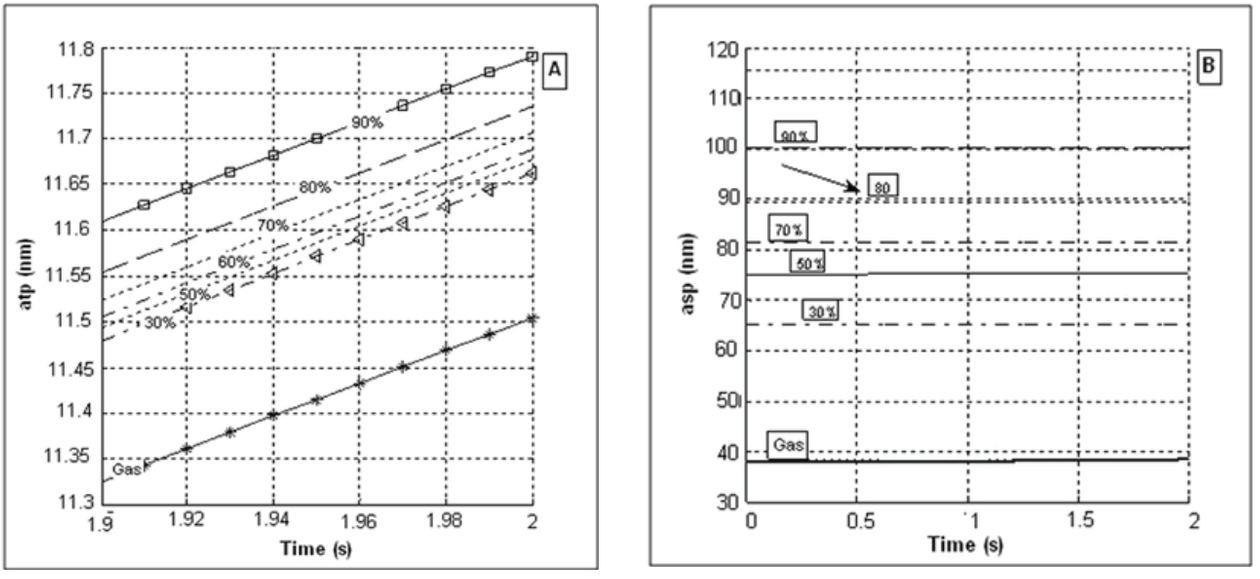

Figure 11: *Geometrical properties of (a) tip-particle, (b) particle-substrate for particle of size* $1\mu m$

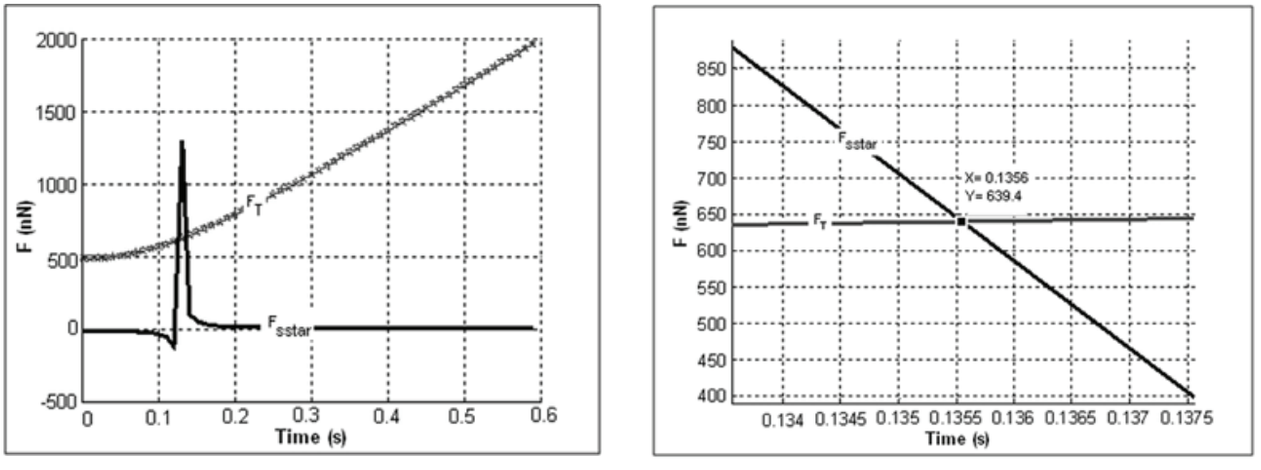

Figure 12: *Transaction of* F_T & F_s^* *curves happened at* $t = 0.1356$ *and* $F_T = 6.395 \times 10^{-7}$ *N.*

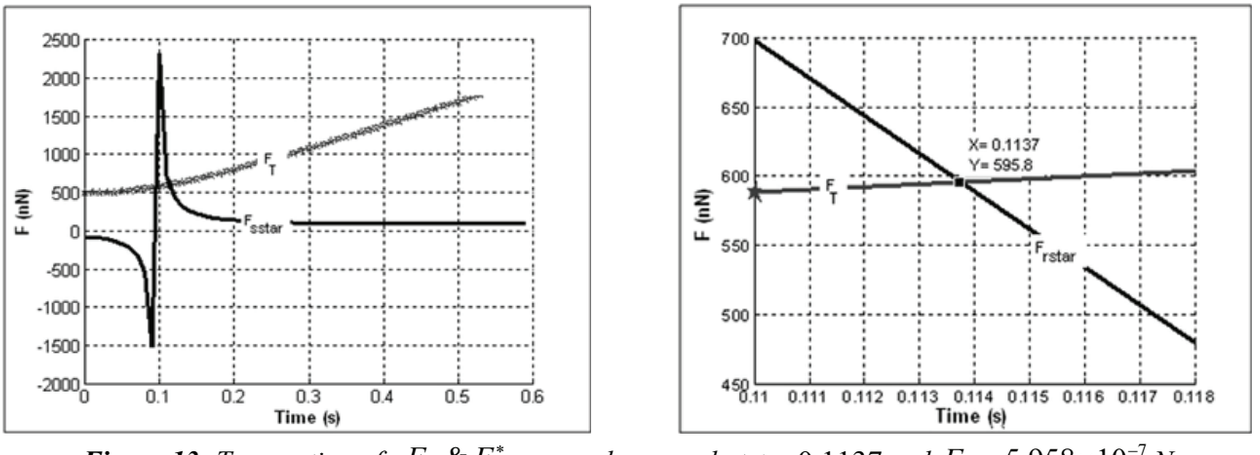

Figure 13: *Transaction of* F_T & F_r^* *curves happened at* $t = 0.1137$ *and* $F_T = 5.958 \times 10^{-7}$ *N.*

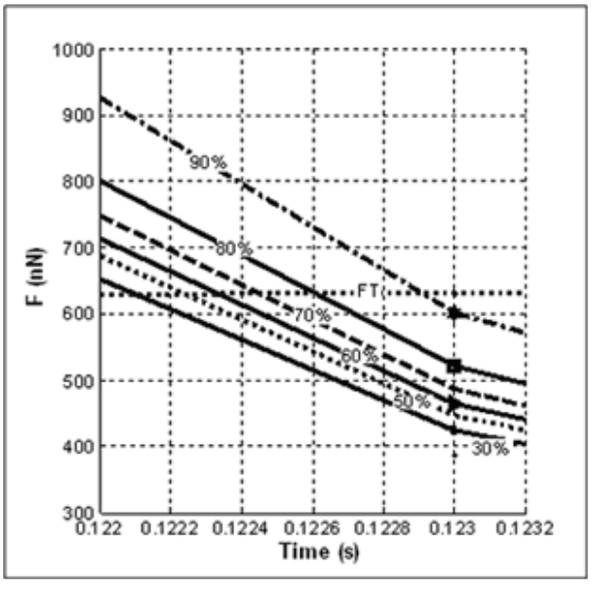

Figure 14: *Growth of humidity percentage and added capillary force makes manipulation and* F_T & F_s^* *intersection point happen with delay.*

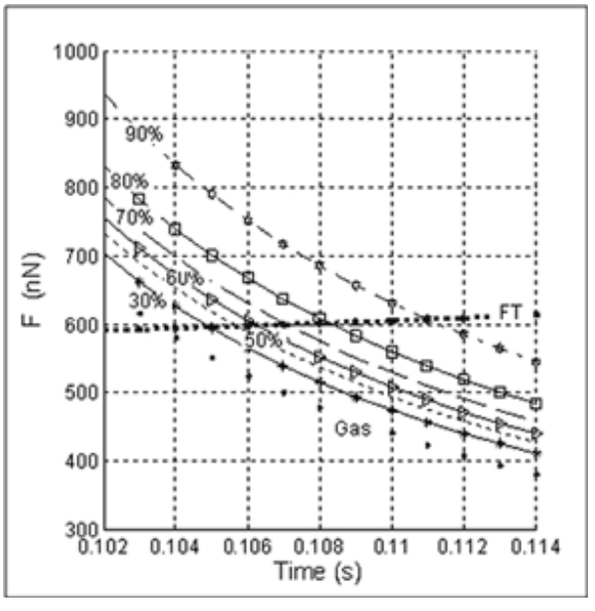

Figure 15: *Growth of humidity percentage and added capillary force makes manipulation and* F_T & F_s^* *intersection point happen with delay.*

Figures 16 and 17 show start point and manipulation force for particles with dimensions of $1\mu m$, $500nm$. As shown, by increasing of nano-particle size the manipulation happens with more delay.

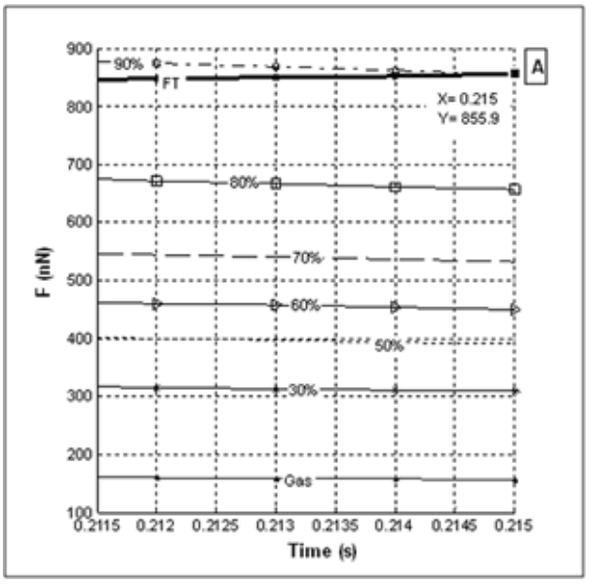

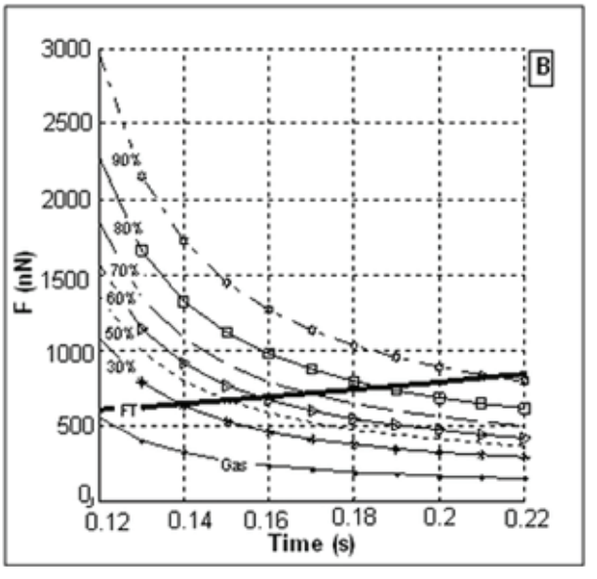

Figure 16: *Time and intersection point of (a)* F_T & F_s^* *and (b)* F_T & F_r^* *for* $500\,nm$ *radius nano-particle*

According to Figures 16 and 17, increasing the particle radius leads to delay in start point. Particle radius growth will make time intervals between different humidity percentages greater and more obvious.

As shown in Figures 18 and 19, intersection point of F_T, F^*_s, F_T, F_r^* increases with humidity percentage growth, as for a $50\,nm$ particle the time has growth of 0.82% for F_s curve and

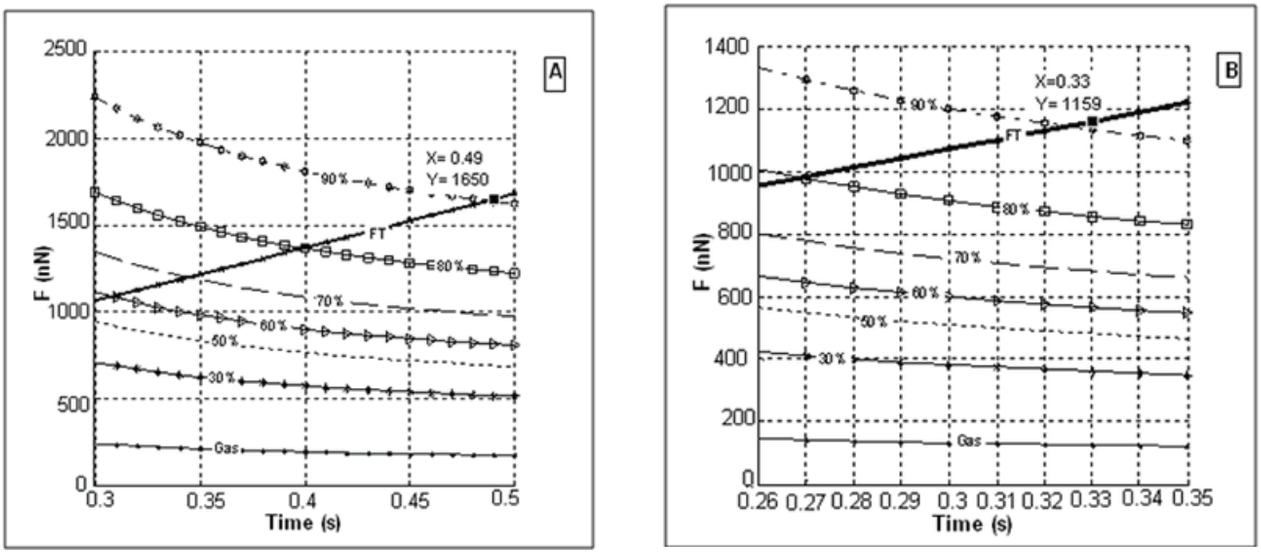

Figure 17: *Time and intersection point of (a) F_T & F_s^* and (b) F_T & F_r^* for $1\mu m$ radius nano-particle*

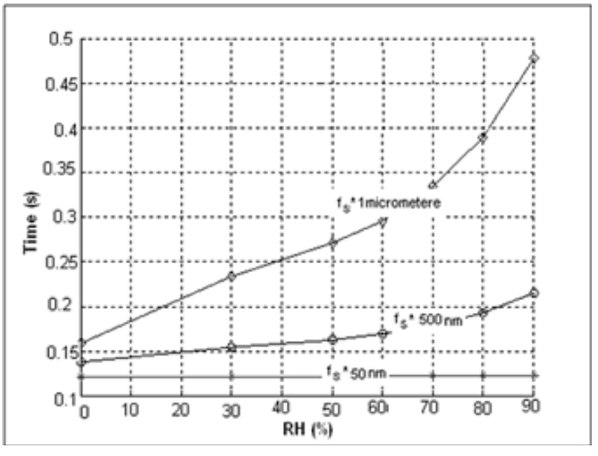

Figure 18: *Comparison between manipulation start point of particles with different radius for F_T^**

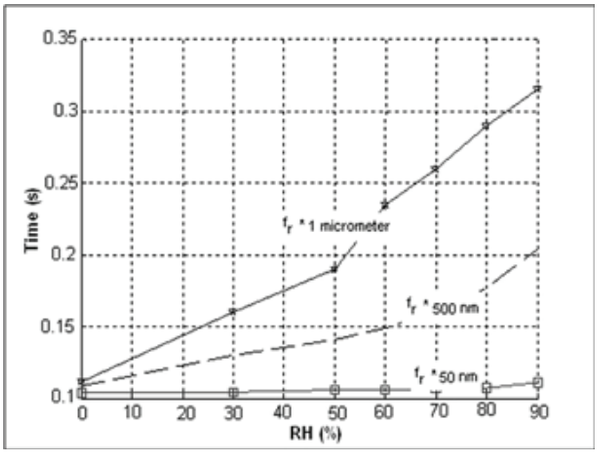

Figure 19: *Comparison between manipulation start points of particles with different radius for F_r^**

7.04% for F_r curve. For a $500\,nm$ particle the time growth is about 55% for F_s curve and 87% for F_r curve. For a $1\,\mu m$ particle these values are 188%,180% respectively for F_s , F_r. As shown in Figure 18, for bigger particles delay rate of manipulation start point is more and in bigger radiuses time difference for different humidity percentage is more obvious.

7. CONCLUSION

Decreasing of particle size to nano-scale changes the situation so much. Some of non-significant forces in macro scale become too important in nano-scale one of which is capillary force. Most of the time calculation of contact area properties such as radius and indentation depth is done regardless

of capillary force, because particles are big in size but for nano-size particles these results are not valid. Since AFM tip used in this research is about 10-20nm in size, the capillary force should be taken into account for accurate calculations. Because DMT model is complicated and Hertz model is not accurate enough, in this paper JKR model has been used to predict contact radius and indentation depth considering the effect of capillary force and humidity percentage. So environmental conditions have been simulated more precisely and consequently dynamic equations and forces have been obtained more accurate. Therefore theoretical results will be closer to experimental ones.

REFERENCES

1. M. Sitti, 2001, "Survey of nanomanipulation systems", IEEE-nano, proceedings of the 1st IEEE Conference on- 0-7803-7215-8.
2. M R. Falvo & R Superfine, "Mechanics and friction at the nanometer scale", J. Nanoparticles, Vol. 2, (2000), pp. 237-248.
3. A. Tafazzoli, M. Sitti, 2004, "Dynamic behavior and simulation of nanoparticles sliding during nanoprobe-based positioning", Proceedings of IMECE'04 2004 ASME International Mechanical Engineering Congress, Anaheim, CA.
4. D.H. Kim, J. Park, B. Kim, K. Kim, 2002, "Modeling and simulation of nanorobotic manipulation with an AFM probe", ICCAS, Muju Resort, Jeonbuk, Korea.
5. S. C. Chen and J. Lin, "Detailed modeling of the adhesion force between an AFM tip anda smooth flat surface under different humidity levels", J. Micromech. Microeng., Vol. 18, (2008), pp. 115006-115013.
6. M. Farshchi Tabrizi, 2007, "On the adhesion between fine particles and nanocontacts: an atomic force microscope study", Doctoral Dissertation, Dep. of Mechanical Engineering, Univ. Siegen.
7. M. Paajanen, J. Katainen, O. H. Pakarinen, A. S.Foster, J. Lahtinen, "Experimental humidity dependency of small particle adhesion on silica and titania", Science Direct Journal of Colloid and Interface Science, Vol. 304, (2006), pp. 518–523.
8. O. H. Pakarinen, A. S. Foster, M. Paajanen, T. Kalinainen, J. Katainen, I. Makkonen, J.Lahtinen and R. M. Nieminen, "Towards an accurate description of the capillary force in nanoparticle-surface interactions", Institute of physics Modeling Simul. Mater. Sci. Eng., Vol. 13, (2005), pp. 1175–1186.
9. L. Sirghi, N.iNakagiri, K. Sugisaki, H Sugimura, and O. Takai, "Effect of Sample Topography on Adhesive Force in Atomic Force Spectroscopy Measurements in Air", Langmuir., Vol. 16, (2000), pp. 7796-7800.
10. K. L. Johnson, K. Kendall, A. D. Roberts, "Surface energy and the contact of elastic Solids", Proceedings of the Royal Society of London. Series A, mathematical and physical sciences, Vol. 324, No. 1558, (1971), pp. 301-313.
11. U.D. Schwarz, "A generalized analytical model for the elastic deformation of an adhesive contact between a sphere and a flat surface", Journal of Colloid and Interface Science, Vol. 261, (2003), pp. 99–106.
12. J. N. Israelachvili, 1991, "Intermolecular and Surface Forces" (London: Academic).
13. M. H. Korayem, M. Taheri, M. Zakeri, "Sensitivity analysis of nanoparticels manipulation based on different friction models", Applied surface science, Vol. 258, (2012), pp. 6713-6722.
14. M. H. Korayem, Z. Rastgar, M. Taheri, "Application of JKR model in manipulation of biological cell: air and liquid environment", Micro and nano letters, Vol. 7, No. 6, (2012), pp. 576-580.
15. R. Jones, H. M. Pollock, J. A. S. Cleaver, Ch. S. Hodges, "Adhesion forces between glass and silicon surfaces in air studied by AFM: Effects of relative humidity, particle size, roughness, and surface treatment", Langmuir, Vol. 18, No. 21, (2002), pp. 8045–8055.